

## Effect of LaAlO<sub>3</sub>-supported modified Ni-based catalysts on aqueous phase reforming of glycerol

Yoon Hwa Park<sup>1</sup> · Ji Yeon Kim<sup>1</sup> · Dong Ju Moon<sup>2</sup> ·  
Nam Cook Park<sup>3</sup> · Young Chul Kim<sup>3</sup>

Received: 26 June 2014 / Accepted: 21 October 2014 / Published online: 21 March 2015  
© Springer Science+Business Media Dordrecht 2015

**Abstract** The present study investigates the catalytic performance over Ni-based catalysts supported on LaAlO<sub>3</sub> perovskite for aqueous phase reforming of glycerol to produce hydrogen. The X–Ni/LaAlO<sub>3</sub> (X = Cu, Co, Fe) catalysts were prepared by precipitation. The amount of added Cu, Fe, and Co in the Ni/LaAlO<sub>3</sub> catalyst was fixed at 5 wt.%. The catalytic reaction was tested at 250 °C and 20 bar with a reactant feed of 15 wt.% aqueous glycerol solution (5 mL/h). The modified Ni/LaAlO<sub>3</sub> catalysts were characterized by Brunauer–Emmett–Teller surface area analysis, X-ray diffraction, H<sub>2</sub>-temperature programmed reduction, H<sub>2</sub>-chemisorption, X-ray photoelectron spectroscopy, and transmission electron microscopy. The morphology and carbon deposition of used catalysts were examined by scanning electron microscopy and thermo-gravimetric analysis, respectively. The Cu–Ni/LaAlO<sub>3</sub> catalyst showed the highest glycerol conversion and hydrogen selectivity, a result attributed to the synergistic effect of the nickel and copper components in the catalyst. The small size and high dispersion of Ni particles and suppressed carbon deposition in the Cu–Ni/LaAlO<sub>3</sub> catalyst positively influenced its catalytic performance.

---

✉ Young Chul Kim  
youngck@jnu.ac.kr

Dong Ju Moon  
djmoon@kist.re.kr

<sup>1</sup> Department of Advanced Chemicals and Engineering, Chonnam National University, 77 Yongbong-ro, Gwangju 500-757, Republic of Korea

<sup>2</sup> Korea Institute Science and Technology, Hwarangno 14-gil 5 Seongbuk-gu, Seoul 136-791, Republic of Korea

<sup>3</sup> Faculty of Applied Chemical Engineering and the Research Institute for Catalysis, Chonnam National University, 300 Yongbong-ro, Gwangju 500-757, Republic of Korea

**Keywords** Glycerol · Aqueous phase reforming · Perovskite · Hydrogen production · Bimetallic catalysts

## Introduction

In recent years, alternative energy resources have become increasingly important owing to dwindling petroleum reserves and increasing environmental concerns associated with fossil fuel utilization. Catalytic conversion of the bio-diesel by-product glycerol into hydrogen is one of the most attractive ways to utilize glycerol and increase its value. Various methods for the production of hydrogen from glycerol exist, which include: (1) steam reforming, a catalytic process that uses steam to obtain a syngas containing hydrogen; (2) partial oxidation through a glycerol catalytic reforming process, using oxygen to acquire hydrogen gas; (3) auto-thermal reforming, which combines steam reforming and partial oxidation reforming; (4) aqueous phase reforming, using glycerol for hydrogen production; (5) supercritical reforming, using critical temperature and pressure to acquire hydrogen gas; and so on. Among these, aqueous phase reforming is the only liquid phase process; all the other available technologies of hydrogen production involve gas phase processes. Aqueous phase reforming has many advantages: for example, it can be performed at a lower temperature than other reforming processes, thus reducing the energy expense, and it produces less CO [1–5]. Ni-based catalysts have been considered as highly effective catalysts for increasing glycerol conversion and hydrogen selectivity like novel catalysts. In Ni-based catalysts, Cu, Co, and Fe are usually used as promoters because they can reduce carbon deposition, which is a cause of deactivation, by providing oxygen to the surface and increasing thermal stability [6–8].

This study investigates the improvement of catalytic activity of Ni/LaAlO<sub>3</sub> catalysts, promoted with Cu, Co and Fe, for the aqueous phase reforming of glycerol.

## Experimental

### Catalyst preparation

LaAlO<sub>3</sub> perovskite was prepared by a citric acid method. The molar ratio of La(NO<sub>3</sub>)<sub>3</sub>·6H<sub>2</sub>O:Al(NO<sub>3</sub>)<sub>2</sub>·6H<sub>2</sub>O: C<sub>3</sub>H<sub>4</sub>(OH)(COOH)<sub>3</sub>: HOCH<sub>2</sub>CH<sub>2</sub>OH was 1: 1: 3: 3. We prepared La(NO<sub>3</sub>)<sub>3</sub>·6H<sub>2</sub>O, Al(NO<sub>3</sub>)<sub>2</sub>·6H<sub>2</sub>O, ethylene glycol and citric acid. Then we mixed all the prepared solutions and stirred at 65–75 °C for 7 h. After stirring, the mixture phase turned into sol phase. After 7 h from the sol phase, its phase changed to gel phase with bubbling. We dried it in the oven overnight and crushed it to make powder above 35 mesh size. We obtained LaAlO<sub>3</sub> perovskite by calcining at 400 °C for 2 h, then 850 °C for 11 h in air condition.

The X–Ni/LaAlO<sub>3</sub> (X = Cu, Co, Fe) catalysts with 15 wt.% Ni and 5 wt.% Cu, Co, and Fe were prepared by the precipitation method. We used Na<sub>2</sub>CO<sub>3</sub> as precipitant. The precipitate was stirred at 80 °C for 1 h and then repeatedly washed. The prepared sample was filtered with distilled water and dried at 110 °C overnight in an oven. All the synthesized catalysts were calcined at 500 °C for 5 h in air.

## Catalyst characterization

The catalysts were characterized by X-ray diffraction (XRD; DMAX100, Cu-K $\alpha$ , Ni filter; Rigaku, Japan), scanning electron microscopy (SEM; JSM-5400A; JEOL), transmission electron microscopy (TEM; JEN-2000FXII; JEOL), BET (ASAP2020; Micromeritics Ins, USA), H<sub>2</sub>-chemisorption and TPR (Chemisorption Analyzer, BEL-CAT; BEL, Japan).

## Catalytic reaction

Aqueous-phase reforming of glycerol was carried out at high pressure in a fixed-bed reactor. The experimental setup consists of a tubular reactor of stainless steel (i.d. = 16 mm,  $L$  = 400 mm). The temperature inside the reactor is measured by a thermocouple located on the catalyst bed. Prior to the reaction, 1 g of the prepared catalyst was reduced in situ at 550 °C for 2 h in a mixture of H<sub>2</sub> (3 mL/min) and Ar (27 mL/min). The catalytic reaction was tested at 250 °C and 20 bar with a reactant feed of 15 wt.% aqueous glycerol solution (5 mL/h). The product stream was separated into a liquid phase and a gas phase component in a condenser connected to the reactor outlet. The gaseous products were analyzed on-line by gas chromatography using a Shimadzu-14B model equipped with a thermal conductivity detector (TCD). The gases H<sub>2</sub>, CH<sub>4</sub>, CO, and CO<sub>2</sub> were separated in a Hayesep D column ( $\Phi$  1/8"  $\times$  7 m, 100/20 mesh) using Ar as the carrier gas.

The conversion of glycerol to gaseous products was calculated according to the following equation on the basis of carbon balance:

$$\begin{aligned} &\text{Glycerol conversion into gaseous products (\%)} \\ &= \frac{\text{C atoms in gas products}}{\text{Total C atoms in the feedstock}} \times 100 \end{aligned} \quad (1)$$

$$\text{H}_2 \text{ selectivity (\%)} = \frac{\text{Produced H}_2 \text{ mol}}{\text{Total glycerol mole converted}} \times \frac{1}{R} \times 100 \quad (2)$$

where  $R$  is the H<sub>2</sub>/CO<sub>2</sub> reforming ratio of 7/3 for glycerol

$$\text{C}_1 \text{ component selectivity (\%)} = \frac{\text{Produced C}_1 \text{ mol}}{\text{Total produced C}_1 \text{ mol}} \times 100 \quad (3)$$

(C<sub>1</sub> component = carbon monoxide, methane, carbon dioxide)

## Results and discussion

### Catalyst characterization

Table 1 shows the BET surface areas of the X–Ni/LaAlO<sub>3</sub> (X = Cu, Co, Fe) catalysts. The Ni/LaAlO<sub>3</sub> catalyst has a lower BET surface area than the X–Ni/LaAlO<sub>3</sub> catalysts. It appears that modification of Ni-based catalysts with Cu, Co,

and Fe increases the BET surface area, indicating that metallic Ni particles are well dispersed on the catalyst surface.

Figures 1, 2 and 3 show the XRD patterns of prepared catalyst in order to identify the structure and particle size of the prepared catalysts. Figure 1 shows a peak at  $2\theta = 33^\circ$ , corresponding to the perovskite structure of all the catalysts. For the X–Ni/LaAlO<sub>3</sub> catalysts, characteristic peaks appeared at  $2\theta = 37.2^\circ$ ,  $43.4^\circ$ , and  $63^\circ$ , corresponding to (111), (200), and (220) of NiO, respectively [9]. No diffraction peaks corresponding to CuO, CeO<sub>2</sub>, and FeO<sub>3</sub> were observed, suggesting that these species were well dispersed on the catalyst surface or had a small particle size. Figure 2 shows the XRD pattern of the reduced catalysts. All the catalysts were completely reduced to metallic Ni<sup>0</sup>, as evidenced by Ni<sup>0</sup> peaks at  $2\theta = 44.5^\circ$  and  $51.8^\circ$ . Figure 3 shows the XRD pattern of the catalysts.

The catalysts still maintained their perovskite structure, and Fe<sub>2</sub>O and CuO peaks were observed. The Ni/LaAlO<sub>3</sub> and Co–Ni/LaAlO<sub>3</sub> catalysts showed a diffraction peak of graphite carbon at  $2\theta = 26.5^\circ$ . This indicates that the lower catalytic activity of the Ni/LaAlO<sub>3</sub> and Co–Ni/LaAlO<sub>3</sub> catalysts is a result of graphite carbon deposition, which causes deactivation of the catalysts.

The crystallite sizes of metallic Ni in the used catalysts were determined using the Scherrer equation. As shown in Table 2, the Ni particle size in the Cu–Ni/LaAlO<sub>3</sub> catalyst was the lowest (10.75 nm), whereas the Ni particle size in Ni/LaAlO<sub>3</sub> was the largest (26.45 nm). We suggest that promotion by Cu, Fe, or Co of Ni supported on a perovskite catalyst has an effect on the metallic Ni dispersion. Table 2 also shows the metallic Ni dispersion of the catalysts measured by H<sub>2</sub>-chemisorption. It can be seen that the Cu–Ni/LaAlO<sub>3</sub> catalyst has the highest Ni dispersion, indicating that there are more active sites present on the Cu–Ni/LaAlO<sub>3</sub> catalyst surface.

Figure 4 shows the TPR profiles of the prepared catalysts. The Ni/LaAlO<sub>3</sub> catalyst exhibited a reduction peak at low temperatures (350 °C), which can be attributed to the reduction of NiO species on the catalyst surface [10, 11]. The presence of the low-temperature reduction peak (200 °C) for the Cu–Ni/LaAlO<sub>3</sub> catalyst indicates the reduction of CuO species. The high temperature reduction peak at 280 °C can be attributed to the reduction of NiO species on the catalyst surface. Figure 4 shows the presence of at least two peaks in the TPR profiles of the Co–Ni/LaAlO<sub>3</sub> catalyst, indicating the reduction of CoO at a lower temperature (300 °C) [12]. The peak at around 489 °C can be attributed to the reduction of Fe<sup>3+</sup> to Fe<sup>2+</sup> in iron oxides [13, 14]. No reduction peak of NiO appeared for the Fe–Ni/LaAlO<sub>3</sub> catalyst, suggesting that the reduction peak of NiO and the reduction peak of Fe<sup>3+</sup> to Fe<sup>2+</sup> in iron oxides overlapped to form one broad peak. The Cu–Ni/

**Table 1** BET surface areas of modified Ni/LaAlO<sub>3</sub>, Ni–Cu/LaAlO<sub>3</sub>, Ni–Co/LaAlO<sub>3</sub>, Ni–Fe/LaAlO<sub>3</sub> catalysts

Catalyst	BET (m <sup>2</sup> /g)
Ni/LaAlO <sub>3</sub>	5.3
Ni–Cu/LaAlO <sub>3</sub>	11.6
Ni–Co/LaAlO <sub>3</sub>	7.1
Ni–Fe/LaAlO <sub>3</sub>	24.1

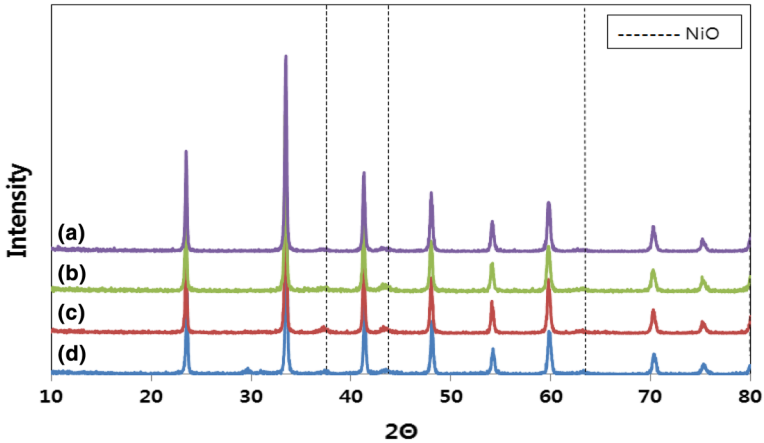


**Fig. 1** XRD patterns of bimetallic catalysts after calcination: *a* Ni-Fe/LaAlO<sub>3</sub>, *b* Ni-Cu/LaAlO<sub>3</sub>, *c* Ni-Co/LaAlO<sub>3</sub>, *d* Ni/LaAlO<sub>3</sub>

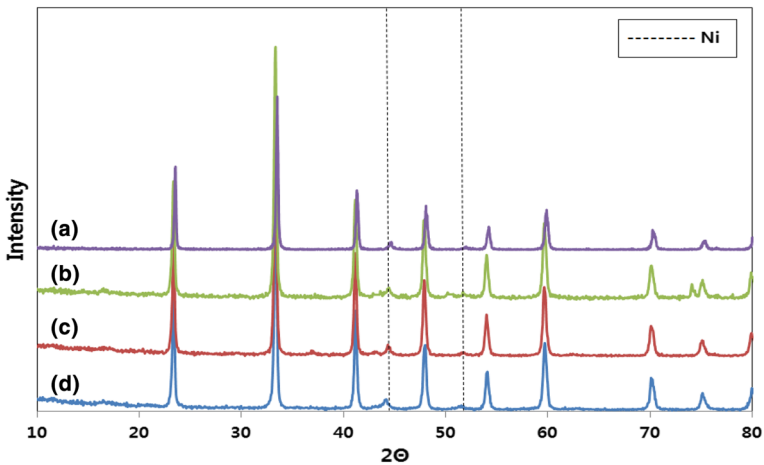


**Fig. 2** XRD patterns of bimetallic catalysts after reduction: *a* Ni-Fe/LaAlO<sub>3</sub>, *b* Ni-Co/LaAlO<sub>3</sub>, *c* Ni-Cu/LaAlO<sub>3</sub>, *d* Ni/LaAlO<sub>3</sub>

LaAlO<sub>3</sub> catalyst showed a lower reduction temperature of NiO than the Ni/LaAlO<sub>3</sub> catalyst. It can be seen that the Cu-Ni/LaAlO<sub>3</sub> catalyst had an enhanced metallic Ni dispersion due to the addition of Cu. Therefore, the Cu-Ni/LaAlO<sub>3</sub> catalyst showed the best reducibility of NiO, which has an effect on the catalytic activity.

The performance of the catalysts in terms of coke formation was compared by thermo-gravimetric analysis (TGA) (Fig. 5). The Co-Ni/LaAlO<sub>3</sub> catalyst shows the lowest level of carbon deposition, whereas the Ni/LaAlO<sub>3</sub> catalyst shows the highest level. The Cu-Ni/LaAlO<sub>3</sub> catalyst shows an intermediate amount of carbon deposition, but shows the best performance in terms of catalytic activity. It is

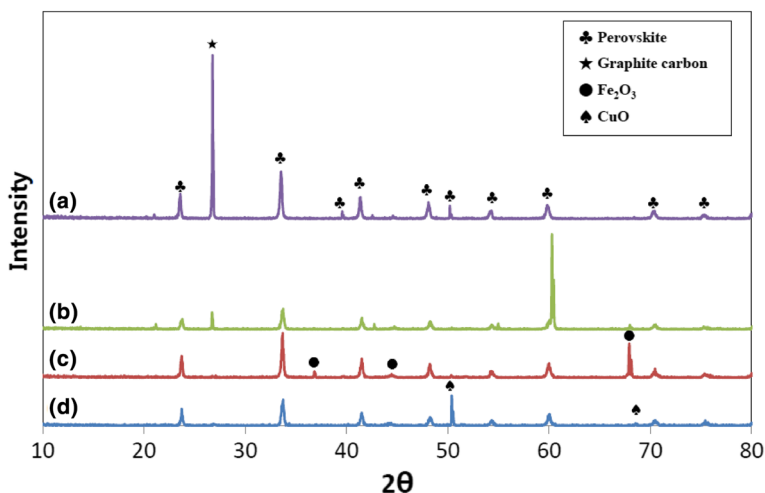


**Fig. 3** XRD patterns of bimetallic catalysts after reaction: *a* Ni/LaAlO<sub>3</sub>, *b* Ni–Co/LaAlO<sub>3</sub>, *c* Ni–Fe/LaAlO<sub>3</sub>, *d* Ni–Cu/LaAlO<sub>3</sub>

**Table 2** Physicochemical properties of the catalysts

Catalyst	NiO diameter (nm) <sup>a</sup>	Ni diameter (nm) <sup>a</sup>	Metal dispersion (%) <sup>b</sup>
Ni/LaAlO <sub>3</sub>	20.83	26.45	0.106
Cu–Ni/LaAlO <sub>3</sub>	29.26	10.75	0.141
Co–Ni/LaAlO <sub>3</sub>	70.61	24.10	–
Fe–Ni/LaAlO <sub>3</sub>	25.66	13.30	–

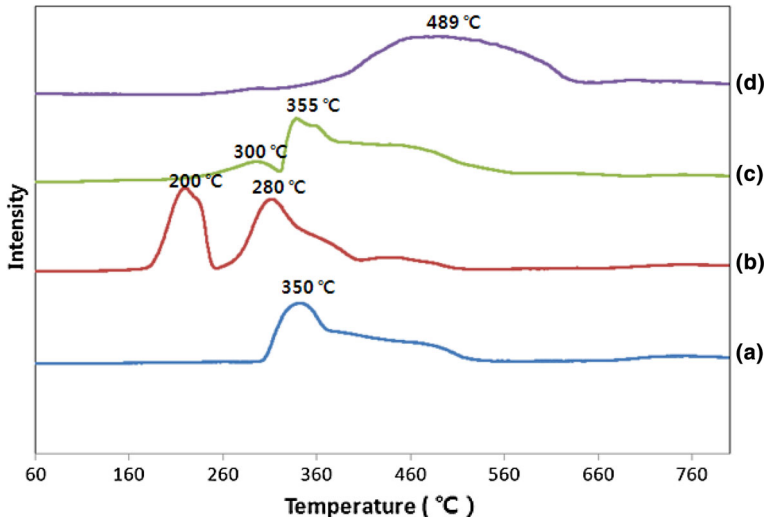
<sup>a</sup> Size of Ni particles on the catalysts determined by the Scherrer equation

<sup>b</sup> Determined from H<sub>2</sub> uptake on the catalysts

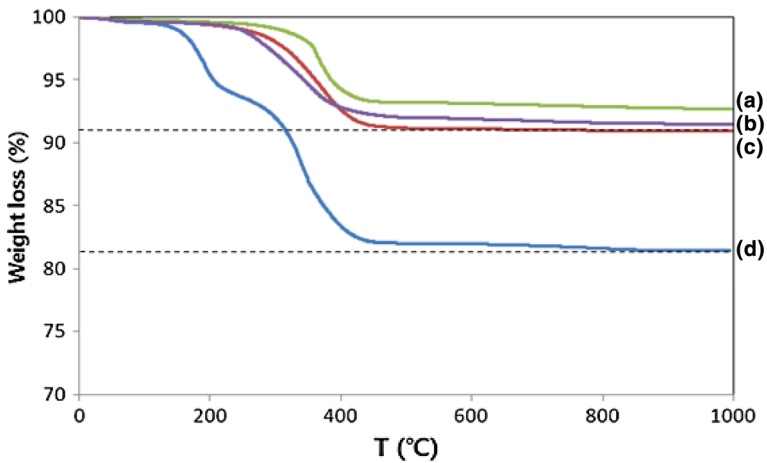
suggested that graphite deposition has a greater influence on the deactivation of the catalyst than the deposition of other forms of carbon or the amount of carbon deposition. The characterization of the XRD patterns shows that whisker-type carbon does not have an effect on the deactivation of catalyst [15, 23].

Figure 6 shows SEM images of fresh and used catalysts. Before reaction, the metal was well supported on the perovskite and the metal particles were dispersed as small clusters of various shapes. After reaction, the Ni/LaAlO<sub>3</sub> catalyst in particular showed higher metallic Ni particle sizes than Ni-based catalysts promoted by Co, Cu and Fe, due to sintering of Ni particles during the aqueous phase reforming. However, no change in the size of the Ni particles on the surface of the Cu–Ni/LaAlO<sub>3</sub> catalyst was observed.

Figure 7 shows TEM images of fresh and used catalyst. Before reaction, the metal particles were well dispersed on the support with small and large particles, respectively. After reaction, the Ni/LaAlO<sub>3</sub> catalyst showed deposition of graphite-type carbon. In contrast, the Cu–Ni/LaAlO<sub>3</sub> catalyst had deposition of whisker-type carbon. According to the literature, the whisker-type carbon does not affect the



**Fig. 4** TPR profiles of catalysts: *a* Ni/LaAlO<sub>3</sub>, *b* Ni-Cu/LaAlO<sub>3</sub>, *c* Ni-Co/LaAlO<sub>3</sub>, *d* Ni-Fe/LaAlO<sub>3</sub> catalysts



**Fig. 5** TGA profiles of catalysts (air, 10–1000 °C): *a* Co-Ni/LaAlO<sub>3</sub>, *b* Fe-Ni/LaAlO<sub>3</sub>, *c* Cu-Ni/LaAlO<sub>3</sub>, *d* Ni/LaAlO<sub>3</sub> catalysts

catalytic performance because it grows on one side of the metallic Ni particles, unlike graphite-type carbon [23].

The surface composition and the oxidation state of metals in the Cu-Ni/LaAlO<sub>3</sub> catalyst before and after reaction were characterized by XPS. Figure 8 shows the XPS spectra of the fresh catalyst. The binding energies of Ni in the Cu-Ni/LaAlO<sub>3</sub> catalyst correspond to that of Ni<sup>2+</sup> (855.75 eV) and Ni<sup>0</sup> (853.60 eV), respectively. After reaction, the binding energy of Ni decreased from its original value of

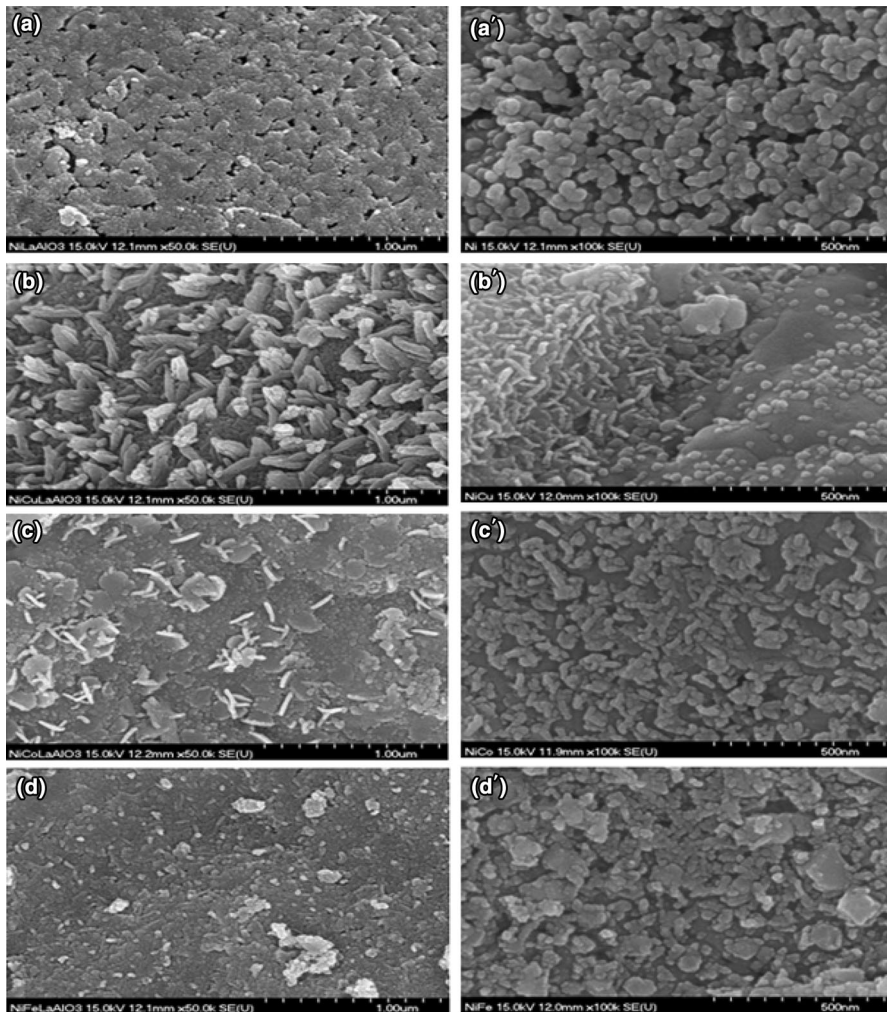


**Fig. 6** SEM images of Ni/LaAlO<sub>3</sub>, Cu–Ni/LaAlO<sub>3</sub>, Fe–Ni/LaAlO<sub>3</sub>, Co–Ni/LaAlO<sub>3</sub> catalysts: (1) Ni/LaAlO<sub>3</sub> **a** before and **a'** after reaction, (2) Cu–Ni/LaAlO<sub>3</sub> **b** before and **b'** after reaction, (3) Fe–Ni/LaAlO<sub>3</sub> **c** before and **c'** after reaction, (4) Co–Ni/LaAlO<sub>3</sub> **d** before and **d'** after reaction

853.08–852.35 eV and the peak in the bimetallic catalyst was intensified. This peak corresponds to the Ni<sup>2+</sup> species and is close to the binding energy of Ni<sub>2</sub>P<sub>3/2</sub> in NiAl<sub>2</sub>O<sub>4</sub>. This peak originates as a result of the decrease in the binding energy of Ni after the reaction; it appears that more Ni atoms are reduced to metallic Ni on the catalyst surface. Figure 8b, b' shows the O<sub>2</sub> XPS spectra of the fresh catalyst. The binding energy of O<sup>-1</sup>s before reaction has contribution from two components: the lower binding energy of 529 eV is attributed to lattice oxygen O<sup>2-</sup> and the remainder is attributed to absorbed O<sub>2</sub><sup>2-</sup>/O<sup>-</sup>, OH<sup>-</sup> of hydroxyl species or oxygen species from a carbonate CO<sub>3</sub><sup>2-</sup> [17–22]. The amount of lattice oxygen before and



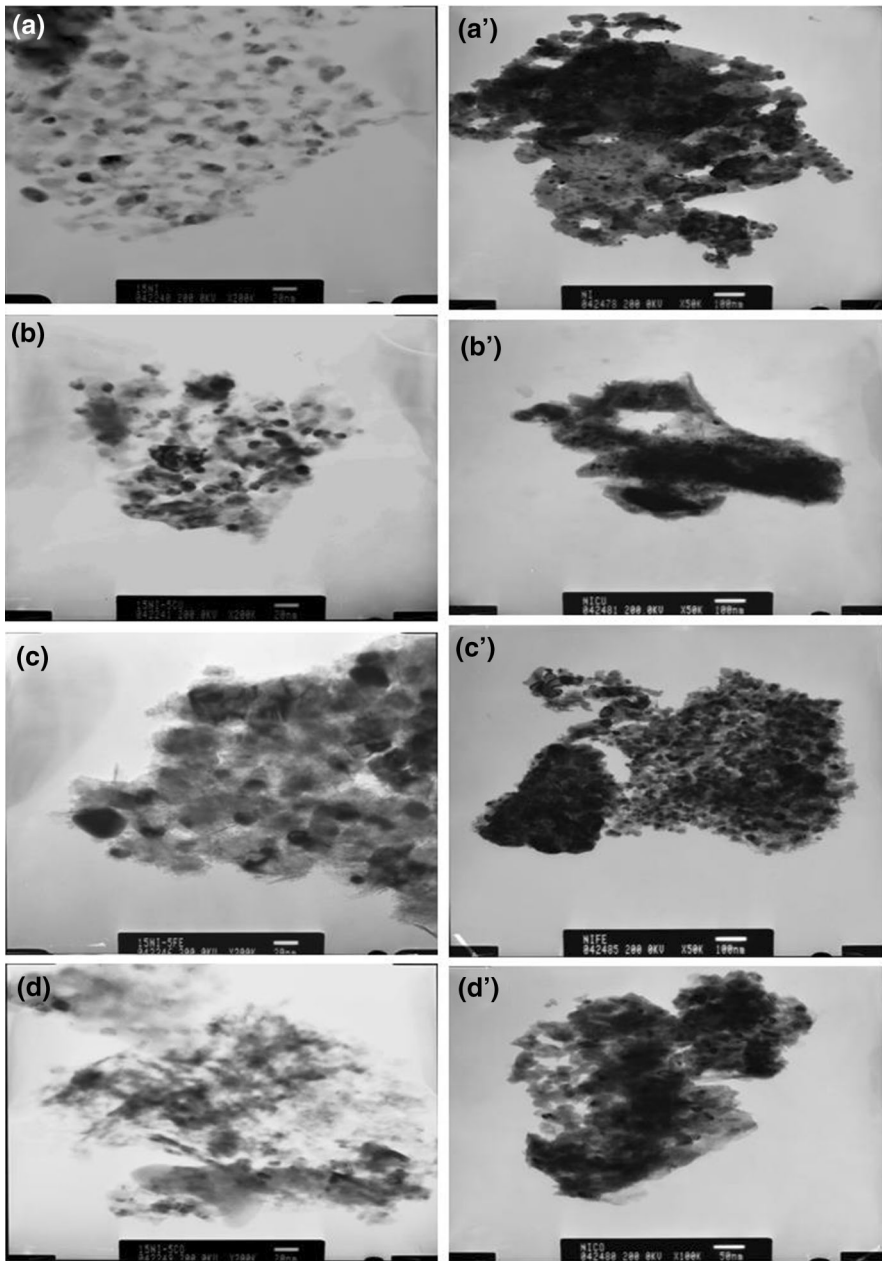


**Fig. 7** TEM images of Ni/LaAlO<sub>3</sub>, Cu-Ni/LaAlO<sub>3</sub>, Fe-Ni/LaAlO<sub>3</sub>, Co-Ni/LaAlO<sub>3</sub> catalysts: (1) Ni/LaAlO<sub>3</sub> **a** before and **a'** after reaction, (2) Cu-Ni/LaAlO<sub>3</sub> **b** before and **b'** after reaction, (3) Fe-Ni/LaAlO<sub>3</sub> **c** before and **c'** after reaction, (4) Co-Ni/LaAlO<sub>3</sub> **d** before and **d'** after reaction

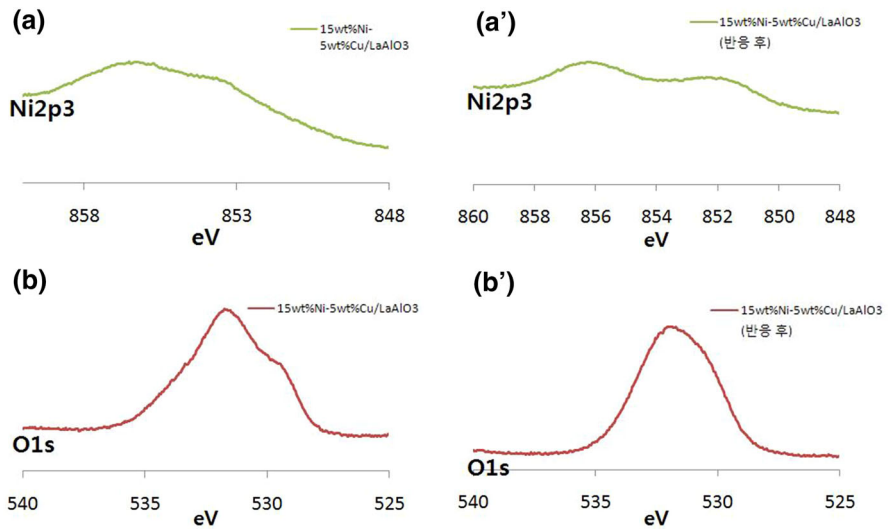


**Fig. 8** XPS analysis of Cu–Ni/LaAlO<sub>3</sub> catalyst before (a, b) and after reaction (a', b')

**Table 3** Glycerol conversion and gas product selectivity (15 wt.% glycerol, 250 °C, 20 bar, 5 mL/h, 1 g catalyst)

Catalyst	Conversion (%)	H <sub>2</sub> selectivity (%)	C <sub>1</sub> compound selectivity (%)		
			CH <sub>4</sub>	CO <sub>2</sub>	CO
15 wt.% Ni/LaAlO <sub>3</sub>	23.4	61.1	10.1	45.4	44.5
15 wt.% Ni–5 wt.% Cu/LaAlO <sub>3</sub>	34.6	79.7	1.4	80.9	17.7
15 wt.% Ni–5 wt.% Co/LaAlO <sub>3</sub>	16.4	64.0	14.1	33.5	52.4
15 wt.% Ni–5 wt.% Fe/LaAlO <sub>3</sub>	27.3	67.6	12.0	44.1	44.0

after reaction was compared, and it was observed that the amount of lattice oxygen is lower after reaction. This indicates that the lattice oxygen content of the Cu–Ni/LaAlO<sub>3</sub> catalyst does not cause a large improvement in resistance to carbon deposition in the aqueous phase process [16–22]. This finding is in agreement with the TGA results, which show that the Cu–Ni/LaAlO<sub>3</sub> catalyst has a relatively large amount of deposited carbon compared to the other catalysts.

### Catalytic activity

The catalytic activities of the catalysts for the aqueous phase reforming of glycerol at 250 °C are shown in Table 3. In the aqueous phase reforming process, measurement was performed at 20 bar and 250 °C with a feed flow rate of 0.083 mL/min (15 wt.% glycerol in water). Glycerol conversion using the Cu–Ni/LaAlO<sub>3</sub> catalyst was found to be 34.6 % and hydrogen selectivity was 79.7 %. Of the catalysts investigated, this catalyst showed the highest glycerol conversion and hydrogen selectivity. The Cu–Ni/

LaAlO<sub>3</sub> catalyst with the smallest Ni particle size and largest BET surface area showed the best catalytic performance, indicating that Ni particle size and BET surface area have an effect on the catalytic performance. The high catalyst activity can also be attributed to the Cu–Ni/LaAlO<sub>3</sub> catalyst presenting a large number of active sites on the catalyst surface. The Cu–Ni/LaAlO<sub>3</sub> catalyst showed the highest carbon dioxide selectivity and the lowest carbon monoxide selectivity. It is suggested that the catalyst favors the water–gas shift reaction and methanation.

## Conclusions

The present work investigated the catalytic performance for aqueous phase reforming of glycerol to produce hydrogen over Ni-based catalysts supported on LaAlO<sub>3</sub> perovskite. The Cu–Ni/LaAlO<sub>3</sub> catalyst showed the highest glycerol conversion and hydrogen selectivity. In addition, the Cu–Ni/LaAlO<sub>3</sub> catalyst showed the highest carbon dioxide selectivity and the lowest carbon monoxide selectivity. It is suggested that this catalyst favors the water–gas shift reaction. The catalytic activity of Cu–Ni/LaAlO<sub>3</sub> was enhanced by the lower metal particle size, the increased number of active sites, and improved Ni dispersion. TEM images of the Cu–Ni/LaAlO<sub>3</sub> catalyst showed the formation of whisker-type carbon during the aqueous phase reforming of glycerol. It is known that the whisker-type carbon has no influence on catalytic activity [23]. The Cu–Ni/LaAlO<sub>3</sub> catalyst was therefore found to be a good catalyst for the aqueous phase reforming of glycerol.

**Acknowledgments** This research was supported by Basic Science Research Program through the National Research Foundation of Korea (NRF) funded by the Ministry of Education (NRF-2009-0094055) and supported partly by the Ministry of Knowledge Economy of Korea and the Korea Institute of Science and Technology (KIST).

## References

1. A.O. Menezes, M.T. Rodrigues, A. Zimmaro, L.E.P. Borges, M.A. Fraga, *Renew. Energy* **36**, 595 (2011)
2. W.B. Kim, G.J. Rodriguez-Rivera, S.T. Evans, T. Voithl, J.J. Einspahr, P.M. Voyles, J.A. Dumesic, *J. Catal* **235**, 327 (2005)
3. R.M. West, E.L. Kunkes, D.A. Simonetti, J.A. Dumesic, *Catal. Today* **147**, 115 (2009)
4. G.W. Huber, J.A. Dumesic, *Catal. Today* **111**, 119 (2006)
5. R.R. Davda, J.W. Shabaker, G.W. Huber, R.D. Cortright, J.A. Dumesic, *Appl. Catal. B* **43**, 13 (2003)
6. C. Wang, B. Dou, H. Chen, Y. Song, Y. Xu, X. Du, L. Zhang, T. Luo, C. Tan, *Int. J. Hydrog. Energy* **38**, 3562 (2013)
7. A. Ebshish, Z. Yaakob, B. Narayanan, A. Bshish, W. Ramli, W. Daud, *Int. J. Integr. Eng.* **3**, 5 (2011)
8. S.Q. Chen, H. Wang, Y. Liu, *Int. J. Hydrog. Energy* **34**, 7995 (2009)
9. R.L. Manfro, A.F.D. Costa, N.F.P. Ribeiro, M.M.V.M. Souza, *Fuel Process. Technol.* **92**, 330 (2011)
10. F. Frusteri, S. Freni, V. Chiode, S. Donato, G. Bonura, S. Cavalloaro, *Int. J. Hydrog. Energy* **31**, 2193 (2006)
11. N.C. Park, W.R. Kim, D.J. Moon, G. Seo, Y.C. Kim, *J. Nanosci. Nanotechnol.* **11**, 1676 (2011)
12. N.J. Luo, K. Ouyang, F.H. Cao, T.C. Xiao, *Biomass Bioenergy* **34**, 489 (2010)
13. L.H. Huang, J. Xie, R.R. Chen, D.R. Chu, W. Chu, A.T. Hsu, *Int. J. Hydrog. Energy* **33**, 7448 (2008)
14. H. Huang, J. Xie, R.R. Chen, D.R. Chu, W. Chu, A.T. Hsu, *Catal. Commun.* **10**, 502 (2009)
15. A.L. Alberton, M.M.V.M. Souza, M. Schmal, *Catal. Today* **123**, 257 (2007)

16. S. Natesakhawat, R.B. Watson, X. Wang, U.S. Ozkan, *J. Catal* **234**, 496 (2005)
17. N.A. Merino, B.P. Barbero, P. Eloy, L.E. Cadus, *Appl. Surf. Sci* **253**, 1489 (2006)
18. R.M. Navarro, M.C. Alvarez-Galvan, J.A. Villoria, I.D. Gonzales-Jimenez, F. Rosa, J.L.G. Fierro, *Appl. Catal. B* **73**, 247 (2007)
19. L. Xi, Z. Hengbin, L. Shujia, C. Feng, Z. Muyu, *Mater. Chem. Phys* **34**, 58 (1993)
20. K. Tabata, Y. Hirano, E. Suzuki, *Appl. Catal. A* **170**, 245 (1998)
21. R. Pereniquez, V.M.G. Delacruz, J.P. Holgado, A. Caballero, *Appl. Catal. B* **93**, 346 (2010)
22. S.S. Lim, D.J. Moon, J.H. Kim, Y.C. Kim, N.C. Park, J.S. Shin, *J. Nanosci. Nanotechnol* **7**, 4013 (2007)
23. J. Rynkowski, P. Samulkiewicz, A.K. Ladavos, P.J. Pomonis, *Appl. Catal. A* **263**, 1 (2004)